Astron. Astrophys. manuscript no.
(will be inserted by hand later)

Your thesaurus codes are:
06 (03.11.1; 16.06.1; 19.06.1; 19.37.1; 19.53.1; 19.63.1)

ASTRONOMY AND ASTROPHYSICS
October 3, 2000

X-ray Spectroscopy of the Cluster of Galaxies Abell 1795 with XMM-Newton

T.Tamura[1], J.S. Kaastra[1], J. R. Peterson[2], F. Paerels[2], J. P.D. Mittaz[3], S. P. Trudolyubov[4], G. Stewart[5], A.C. Fabian[6], R.F. Mushotzky[7], D. H. Lumb[8], and Y. Ikebe[9]

[1] SRON Laboratory for Space Research Sorbonnelaan 2, 3584 CA Utrecht, The Netherlands
[2] Astrophysics Laboratory, Columbia University, 550 West 120th Street, New York, NY 10027, USA
[3] Department of Space and Climate Physics, University College London, Mullard Space Science Laboratory, Holmbury St. Mary, Surrey, U.K.
[4] NIS-2, Los Alamos National Laboratory, Los Alamos, NM 87545, USA
[5] Department of Physics and Astronomy, The University of Leicester, Leicester LE1, UK
[6] Institute of Astronomy, University of Cambridge, Madingley Road, Cambridge, CB3 0HA, UK
[7] NASA Goddard Space Flight Center , Code 662, Greenbelt, Maryland 20771, USA
[8] Astrophysics Div., European Space Agency, ESTEC, Postbus299, 2200AG Noordwijk, The Netherlands
[9] Max Planck Institut für Extraterrestrische Physik, Postfach 1312, 85741 Garching, Germany

Received ?; accepted ?

Abstract. The initial results from XMM-Newton observations of the rich cluster of galaxies Abell 1795 are presented. The spatially-resolved X-ray spectra taken by the European Photon Imaging Cameras (EPIC) show a temperature drop at a radius of $\sim$ 200 kpc from the cluster center, indicating that the ICM is cooling. Both the EPIC and the Reflection Grating Spectrometers (RGS) spectra extracted from the cluster center can be described by an isothermal model with a temperature of $\sim$ 4 keV. The volume emission measure of any cool component ($<$ 1 keV) is less than a few % of the hot component at the cluster center. A strong O VIII Lyman α line was detected with the RGS from the cluster core. The O abundance of the ICM is 0.2–0.5 times the solar value. The O to Fe ratio at the cluster center is 0.5–1.5 times the solar ratio.

Key words: Galaxies: clusters: individual: Abell 1795 – Galaxies: clusters: general – Galaxies: cooling flows – – X-rays: galaxies

1. Introduction

X-ray observations have revealed prominent features around the central galaxy of many galaxy clusters. These include a sharply peaked X-ray emission (Jones and Forman 1984) and a cool plasma component with a temperature less than 2 keV (e.g., Canizares et al. 1982). These should be related to the radiative cooling of the intra-cluster-medium (a cooling flow; Fabian 1994), since the radiative cooling time at the center of these clusters is much less than the cluster age. In order to understand the nature of the cooling of the ICM, more studies on its temperature structure, spatial distribution are necessary.

Send offprint requests to: T.Tamura
Correspondence to: T.Tamura@sron.nl

Here we report the first results from the XMM (Jansen et al. 2001) observations of a rich cluster of galaxies, Abell 1795 (A1795 for short). This cluster, at a redshift of 0.0631, is one of the best targets for measurements of its temperature structure with XMM. This is because of its peaked X-ray emission and a cool (2–4 keV) component at the cluster center (Briel and Henry 1996; Fabian et al. 1994; Fabian et al. 2000). We have measured the temperature structure and metal abundances of the central region based on X-ray spectra with high spectral resolution. Throughout this *Letter*, we assume the Hubble constant to be $H_0 = 50\ h_{50}$ km s^{-1}Mpc^{-1} and use 1σ errors ($\Delta\chi^2 = 2.0$) unless stated otherwise. One arc-minute corresponds to $110 h_{50}^{-1}$ kpc.

2. Observations

XMM observations of A1795 were performed on 2000 June 26 during the performance verification phase. The three EPICs (Turner et al. 2001) were operated in the full window mode with the thin filter. The RGS (den Herder et al. 2001) were operated in the spectroscopy mode. The RGS dispersion axis is oriented along an axis of about -70 degrees (North to East). We report on simultaneous UV/optical observations with the Optical Monitor in another *Letter* (Mittaz et al. 2001).

3. Analysis

Using the EPIC spatially-resolved spectra we have measured large-scale properties of the cluster. Then, utilizing the high resolution RGS spectra we constrain the temperature structure in the cluster core.

For basic data processing, we used the the development version of the Science Analysis System (SAS) for all data. The EPIC and RGS events were screened by rejecting the high background periods. Useful exposure times for EPIC/PN,

EPIC/MOS and RGS are 25 ksec, 34 ksec, and 41 ksec, respectively. The background spectra for these instruments were taken from Lockman-Hole observations and subtracted before the spectral fitting below. The EPIC data were corrected for telescope vignetting. For spectral fitting, we utilize the SPEX (Kaastra et al. 1996) and XSPEC (Arnaud 1996) packages. We model the plasma emission using the MEKAL emission code (Mewe et al. 1995), but with updated wavelengths according to Phillips et al. (1999).

3.1. The EPIC results

We extracted the spectra from the three EPIC detectors separately in annuli around the emission center with outer radius ranging from 8″ to 512″. The emission from the strongest point sources was subtracted from the spectra. The MOS spectra were fitted with an isothermal model. The column density $N_{\rm H}$ was assumed to be the Galactic value of $1.1\,10^{20}\,{\rm cm}^{-2}$. We obtained statistically acceptable fits for all annuli. The obtained temperature, metallicity, and hydrogen density are shown in Fig. 1. The PN spectra were also fitted with the same model. In this case, the $N_{\rm H}$ was left free, in order to constrain absorption due to possible cold gas in the cluster. The fits are statistically acceptable for all annuli and the results are shown in Fig. 1.

These results are consistent among the two instruments, except for temperatures measurements beyond 4′. The difference in the temperature between PN and MOS beyond 4′ may be caused by residual uncertainty in the background subtraction.

The obtained column density from the PN indicates no excess absorption above the Galactic value. Within ∼2′ in radius from the center, the temperature decreases and the metallicity increases towards the center. With the large effective area and moderate spatial resolution of the instrument, we could resolve the ICM structure in sub-arcmin scale for the first time.

For further examination of the central temperature structure, we have fit the MOS spectrum within a radius of 2′ using two thermal components. The temperature of the hot component was consistent with the value obtained for the outer regions. For the cooler component we have obtained good fits using an isothermal component with a temperature of 3–4 keV. Alternatively, we attempted to model the cool component by an isobaric cooling flow model (Johnstone et al. 1992), however in order to obtain a good fit to this model the temperature distribution had to be cut-off at 2.6±0.6 keV. Essentially no cooler gas is seen directly in the EPIC data. The mass deposition rate of the cooling flow was poorly constrained (500–3000 $M_\odot$/year) due to a strong correlation with the emission measure of the hot component. This is due to the relative high cut-off temperature only a factor of 2–3 below the temperature of the hot component. Fits with a very small cut-off temperature did not produce acceptable fits with a $\chi^2 \sim 569$ for 238 degrees of freedom when $kT_{\rm min} = 0.01$ keV.

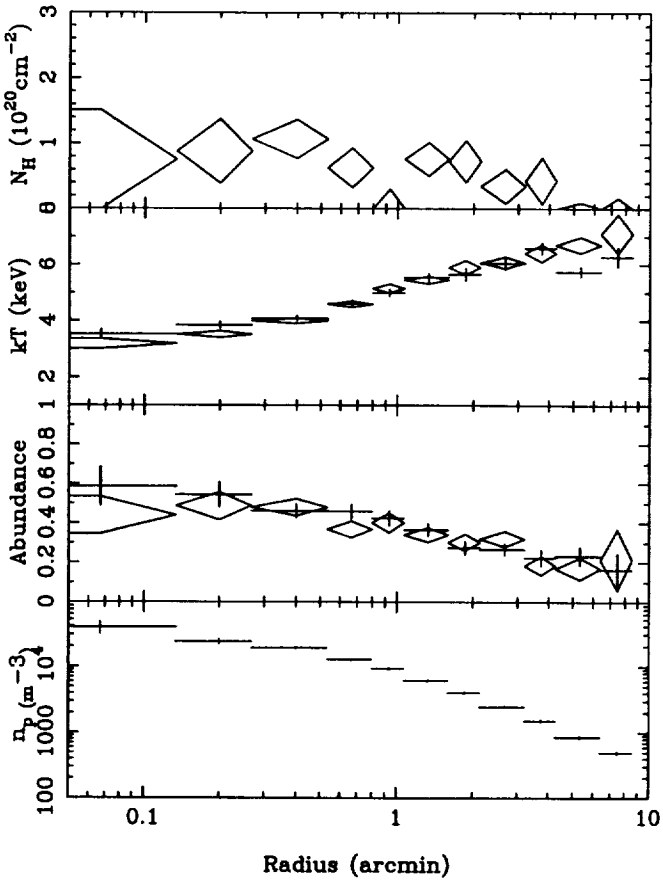

Fig. 1. Properties of the ICM as a function of projected radius derived from the PN and MOS spectra based on a single temperature model. From top to bottom, absorbing column density, temperature, metal abundance, and the deprojected hydrogen density were shown, respectively. The PN and MOS results were shown by diamonds and crosses, respectively.

3.2. The RGS results

The RGS spectra (RGS1 and RGS2) were extracted from the central 1′ in full-width. Because of the principle of the instrument, each spectrum contains emission from a range of different projected positions. Based on the MOS image in the RGS energy band, we estimate that in the central RGS spectrum, more than about 50-60% and 80% of the flux comes from projected radii of $< 30''$ and $< 60''$, respectively. Based on these spectra, we examine the nature of the central region of the cluster. We have detected the O VIII Lyman α line clearly with an intensity of $1.2\,10^{51}$ photons/s. The observed FWHM of the line is about 150 mÅ, which corresponds to a source extent of ∼1′. The measured line wavelength is consistent with a redshift of 0.0631 within the statistical errors (∼ 30 mÅ). The wavelength uncertainty corresponds to a velocity shift of ∼ 500 km sec^{-1}. In addition to the O VIII line, also some line blends in the wavelength range of 11–14 Å are observed. These are mainly due to Fe XXIV (around 10.6Å and 11.2Å), Ne X (12.1Å), and Fe XXIII (12.2Å). These line measurements

Table 1. The isothermal fits to the RGS spectra of the center of A1795. Numbers in parentheses are 1σ confidence uncertainties for one interesting parameter.

Parameter	RGS1	RGS2
EM^a	37	41
$N_{\rm H}^b$	5.0 (3.7–6.2)	2.6 (0.2–4.3)
kT (keV)	3.8 (2.9–5.5)	4.0 (3.1–6.3)
O^c	0.30 (0.20–0.49)	0.30^d
Ne^c	0.66 (0.36–1.3)	0.61 (0.4–1.3)
Fe^c	0.37 (0.23–0.78)	0.36 (0.23–1.0)
χ^2/ν	356/310	222/247

[a] The volume emission measure in units of $10^{72}{\rm m}^{-3}(10^{66}{\rm cm}^{-3})$.
[b] The column density in units of $10^{24}{\rm m}^{-2}(10^{20}{\rm cm}^{-2})$.
[c] Metal abundances relative to the solar values. The solar values are taken from Anders and Grevesse (1989), with O/H= $8.51\,10^{-4}$, Ne/H= $1.23\,10^{-4}$, and Fe/H= $4.68\,10^{-4}$.
[d] Due to the failure of one CCD on RGS2, the O VIII line was not detected with RGS2. Therefore we fixed the O abundance for the RGS2 fit.

should constrain the presence of material with a temperature of 0.5–3 keV.

3.2.1. Isothermal model fitting

The EPIC data showed that the cluster core region is close to being isothermal with a temperature of 3–4 keV. For further examination of this isothermality, we fitted the central RGS spectra with an isothermal model. The effects of a finite source extent were taken into account as follows. We calculated the line spread function based upon the source surface brightness profile and convolved this with the RGS response for a point source. A β model was assumed for the brightness profile. The core radius was a free parameter in the spectral fitting procedure. We limited the wavelength band to 10-23 Å and 10-20 Å for RGS1 and RGS2, respectively, where most of the interesting emission lines are expected, and the estimated background is less than 10% of the source flux.

The fits to RGS1 and RGS2 are statistically acceptable and the best-fit parameters are shown in Table 1. The best-fit parameters from the two detectors are consistent with each other. The RGS spectra and the best-fit model are shown in Fig. 2.

In the RGS1 spectrum, there is line-like structure around 18 Å in observed wavelength. This could be due to line blends from Fe XVII. However, this structure is not seen in the RGS2 spectrum. In addition, the maximum allowed emission measure from these blends, for a temperature of ~ 0.5 keV is on the order of 1% of the total emission measure obtained above. Therefore, we conclude this residual is not significant. Non-statistical noise in background may be the origin of this structure.

The line profiles can be described using a core radius of $20''-30''$ for the assumed brightness profile. This is roughly consistent with the observed X-ray brightness (Xu et al. 1998; Allen 2000).

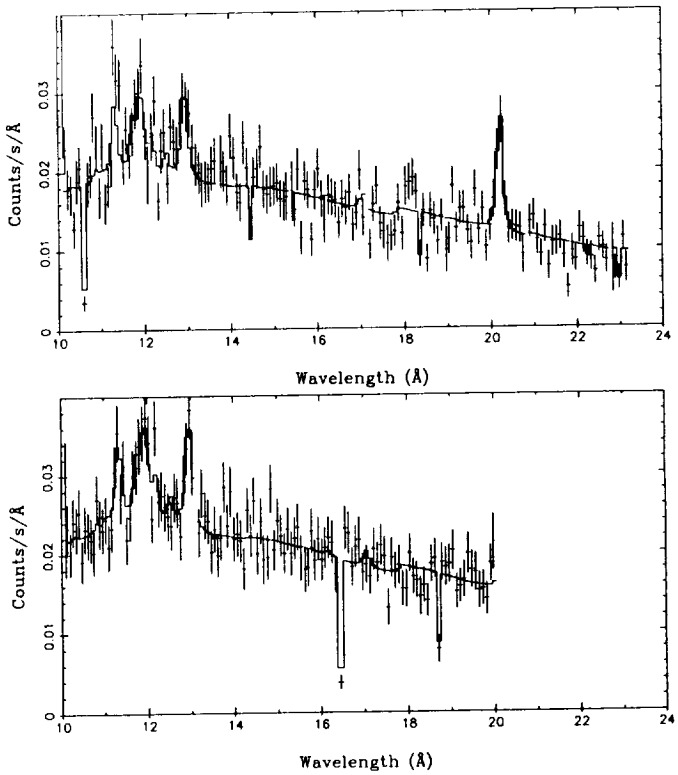

Fig. 2. The spectra extracted from the central region of A1795. The wavelength scales are not corrected for the redshift. Top and bottom panels show the RGS1 and RGS2 spectra, respectively. The data are shown with an isothermal model. Except for the normalization, we plot the models with the average parameters from table.1. Due to CCD gaps and hot pixels, some wavelength bands were not covered by each RGS. These are indicated by gaps and drops in the model spectrum.

The $N_{\rm H}$ value obtained is above the Galactic value as well as the value obtained with the EPIC above. However, the excess $[(2-3)\,10^{20}{\rm cm}^{-2}]$ is within the systematic uncertainty due to the RGS response and the estimated background.

3.2.2. Limits on the cool component

Thus, the RGS spectra do not require an additional cool component with a temperature lower than 3 keV above the isothermal model. Nevertheless, within the central region ($r < 1'-2'$), the cooling time inferred from X-ray observations is much smaller than the possible cluster age (Edge et al. 1992). This suggests the presence of cool material with a range of temperatures. In fact, a recent Chandra observation revealed cool emission (~ 2 keV) around the cD galaxy (Fabian et al. 2000).

In order to constrain the possible cool component, we fitted the data by adding a cooler plasma component in addition to the isothermal model. Firstly, we considered an additional isothermal component. Since the RGS is not so sensitive to hot plasma (> 3 keV) we fixed the hot component temperature $T_{\rm hot}$ to 6.4 keV, the ICM value obtained with the EPIC. The abundances of both components were fixed to 0.4 solar, except for the Ne abundance. The Ne abundance was fixed to

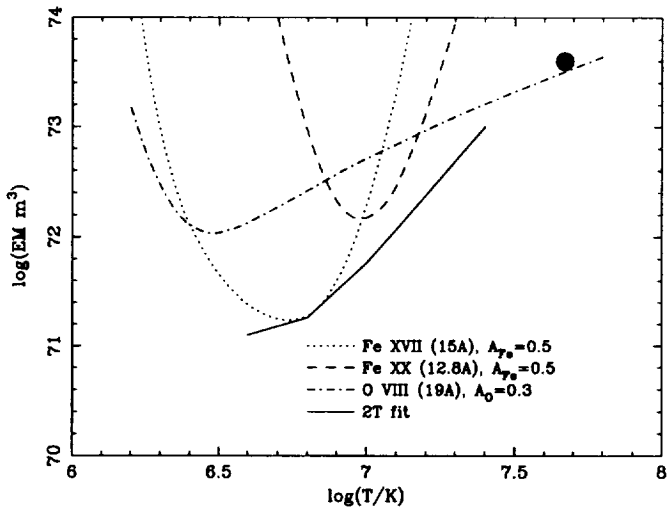

Fig. 3. The volume emission measure ($EM_{\rm cool}$) within a effective radius of 1′ as a function of temperature $T_{\rm cool}$. Each line shows upper limits of $EM_{\rm cool}$ of the *isothermal* cool component based on the upper limit of a line (and line blends) flux and two temperature model fitting. The filled circle indicates the emission measure and temperature of the hot component derived from the isothermal model fit to the RGS spectra. Note that the emission measure depends on the Hubble constant as $\propto h_{50}^{-2}$.

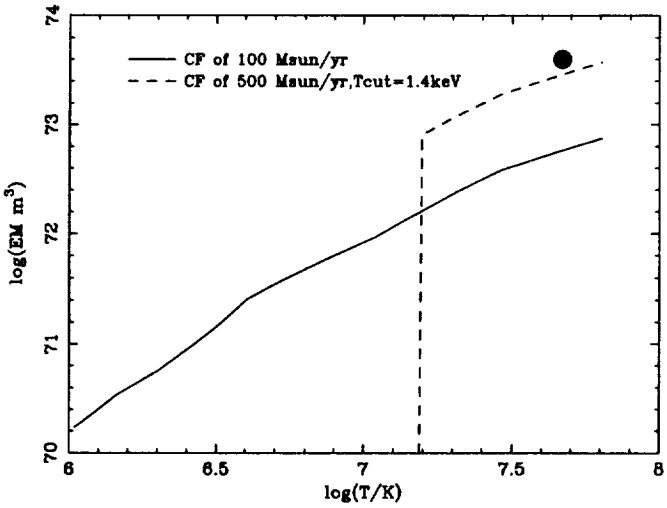

Fig. 4. The cumulative volume emission measure [$EM_{\rm cool}(< T)$] as a function of temperature based on two CF models. The upper limit of the deposition rate $\dot{M}$ is 100-170 $M_\odot$/yr.

0.64 times solar based on the isothermal fits. The $N_{\rm H}$ value was also fixed to $3\,10^{20}{\rm cm}^{-2}$, which is the best-fit value for the isothermal model. We measured the upper limits to the volume emission measure of the cool component, $EM_{\rm cool}$, for a given temperature of the cool component, $T_{\rm cool}$. The emission measure of the hot component, $EM_{\rm hot}$, was left free. The results are shown in Fig. 3. When $T_{\rm cool}$ is below 1.5 keV, $EM_{\rm cool}$ is less than 10% of $EM_{\rm hot}$.

Secondly, we considered a continuous distribution in temperature based on an isobaric cooling flow model (CF; Johnstone et al. 1992). In this model, $EM_{\rm cool}$ was assumed to be

$$\int dEM(T) = \frac{5}{2}\frac{\dot{M}}{\mu m_{\rm p}}\int_{T_{\rm min}}^{T_{\rm max}}\frac{dT}{\Lambda(T)},$$

where $\dot{M}$, μ, and $m_{\rm p}$ are the mass deposition rate, mean molecular weight, and the proton mass, respectively. $\Lambda(T)$ is the cooling function. The temperature of the hot component, $T_{\rm hot}$, the abundances of both components, and $N_{\rm H}$ were fixed to the same values as above. The maximum temperature of the CF, $T_{\rm max}$, was fixed to the same value as $T_{\rm hot}$. This CF component was added to the isothermal component. We found an upper limit to $\dot{M}$ of 110–170 $M_\odot$/yr. When we assume a cooling flow with $\dot{M}$ = 500 $M_\odot$/yr, the lower temperature should be larger than $\sim$ 1.4 keV in order to produce the observed RGS spectra. The cumulative $EM_{\rm cool}$ of the CF model with this upper limit $\dot{M}$ is shown in Fig. 4. Similar to the two temperature model fitting, the emission measure of the cool component is very small compared to that of the hot component.

These tight upper limits were obtained through the lack of emission lines such as Fe XX (12.8 Å in the rest frame) and Fe XVII (around 15 Å and 17 Å) in the observed spectra. In order to constrain the limit more directly and confidently, we focused on particular ionization stages of ions and their line emissions.

The Fe XVII line at a rest wavelength of 15.0 Å is a sensitive indicator of plasma with a temperature of 0.2–0.8 keV. As shown in Fig. 2, the RGS spectrum indicates no significant residual at this wavelength. By adding this line to the isothermal model we derived an upper limit to the line intensity of $1.7\,10^{50}\,h_{50}^{-2}$ photons/s. A further constraint can be derived from the Fe XX blends at a rest frame wavelength of 12.8 Å. This is sensitive to a temperature of 0.5–2.0 keV. The upper limit to the Fe XX blends is $4.2\,10^{50}\,h_{50}^{-2}$ photons/s.

These line measurements place limits on the presence of cool component(s) without assumptions above on the temperature structure and the detailed emission model. We calculate $EM_{\rm cool}$ based on the line intensities measured above for a given $T_{\rm cool}$ and metallicity, following Canizares et al. (1982). The result is shown in Fig. 3. The predicted emission measure based on the line intensity of the O VIII line is also shown, for reference. Here we assumed an O and Fe abundance of 0.3 and 0.5 solar, respectively, based on our measurement. The emission measure of the possible cool component is less than 10% of that of the hot component within the central volume when $T_{\rm cool}$ is below 1 keV.

When we assumed the isobaric cooling flow model for $EM_{\rm cool}$, the limits for Fe XVII correspond to $\dot{M}$ = 100 $M_\odot$/yr. This is similar to the value obtained above based on the spectral fitting, indicating that $\dot{M}$ is strongly constrained by a lack of the Fe XVII lines in the spectra.

3.2.3. Oxygen abundance

The abundance of O and its ratio to other elements in the ICM strongly depends on its origin. Nevertheless, previous measurements of the O abundance had a large uncertainty (e.g. Canizares et al. 1982), except for a few cases (e.g., Matsumoto et al. 1996). This is not only because of the limited sensitivity to O lines but also because of uncertainty in the temperature structure of the ICM. We detected the O VIII Lyman α line clearly for the first time in this cluster and we constrained the temperature structure tightly. This provides a good opportunity to measure the O abundance.

As shown in Table 1, the isothermal fits to the RGS data yielded an O abundance of 0.2–0.5. When we used the central ICM temperature of 4.5 keV determined by EPIC, the O abundance is 0.27–0.47 solar.

4. Summary and Discussion

Based on the XMM observations of Abell 1795, we have obtained the following results.

The temperature and metallicity of the ICM are radially uniform at radii from 2′–8′ [$\sim$ $(200 - 800)\, h_{50}^{-1}$ kpc], with an observed temperature of 6–7 keV and metallicity of 0.2–0.3 solar. This confirms the previous idea that the cluster is close to being dynamically relaxed (e.g., Briel and Henry 1996).

Below a radius of $\sim$ 2′ the effective temperature of the ICM starts to decrease towards the center. Except inside the central 1′ the observed temperature profile agrees well with that obtained from a deprojection analysis based on the cooling flow model (Edge et al. 1992). Using the deprojection technique and assuming a cooling time of a Hubble time and a flat central potential, Edge et al. obtained a mass deposition rate of $\sim 500\ M_\odot$/year.

The EPIC and RGS spectra extracted from the cluster center ($r < 30''$–$60''$) can be described by an isothermal model with a temperature of $\sim$ 4 keV. The volume emission measure of cool component ($\sim$ 1 keV) was found to be less than a few % of the hot component at the cluster center, through the absence of clear Fe XVII and Fe XX line emission in the RGS spectra. This is significantly smaller than the cooling flow prediction (Edge et al. 1992). In fact, isobaric cooling flow models with $\dot{M}$ of $\sim 500\ M_\odot$/yr predict more flux from Fe XVII – Fe XX than our measurements. The absence of these emission line is difficult to model with a uniform absorber and we derive a covering fraction of $< 10\%$ for gas of sufficient column density (10^{21} cm^{-2}) necessary to "hide" the iron lines. The absence of the cool emission is also supported by the cut-off temperature of $\sim$2.5 keV found by fitting cooling flow models to the EPIC data. We derived an upper-limit to $\dot{M}$, of $100 - 170\ M_\odot$/yr, which is smaller than found by Allen et al. (2000; $250 \pm 30\ M_\odot$/yr) based on the ASCA and ROSAT data.

Our results for A 1795 are very similar to what has been found in A 1835 (Peterson et al. 2001) and Sérsic 159-03 (Kaastra et al. 2001). A full discussion of possible explanations for the lack of observed cool gas is given by Peterson et al. (2001) in their analysis of the A 1835 cluster.

We detected the O VIII Ly α line from the cluster center with the RGS. The O abundance was found to be 0.2–0.5 solar value. This is similar to the value obtained in the center of the Virgo cluster (Matsumoto et al. 1996) based on ASCA spectra, and in the centers of A 1835 (Peterson et al. 2001) and Sérsic 159-03 (Kaastra et al. 2001) based on XMM/RGS spectra. The O to Fe ratio at the cluster center is $0.5 - 1.5$ times the solar ratio. Since oxygen and iron are mainly produced in type II and Type Ia supernovae, respectively, the observed ratio suggests significant contributions from both type Ia and type II to the metal enrichment at the cluster center. In the core the Fe abundance is a factor of 2 larger than in the outer parts (see Fig. 1). This is consistent with the general idea that the iron abundance is higher around the cD galaxy (Fukazawa 1998; Fukazawa et al. 2000).

Acknowledgements. This work is based on observations obtained with XMM-Newton, an ESA science mission with instruments and contributions directly funded by ESA Member States and the USA (NASA). The Laboratory for Space Research Utrecht is supported financially by NWO, the Netherlands Organization for Scientific Research.

References

Allen, S.W., 2000, MNRAS 315, 269
Allen, S.W., Fabian, A.C., Johnstone, R.M., et al 2000, submitted to MNRAS (astro-ph/9910188)
Anders, E., Grevesse, N., 1989, Geochim. Cosmochim. Acta 53, 197
Arnaud, K.A., 1996, Astronomical Data Analysis Software and Systems V, eds. Jacoby G. and Barnes J., p17, ASP Conf. Series volume 101.
Briel, U.G., Henry, J.P., 1996, ApJ, 472, 131
Canizares, C.R., Clark, G.W., Jernigan, J.G., Markert, T.H., 1982, ApJ 262, 33
Edge, A.C., Stewart, G.C., Fabian, A.C. , 1992, MNRAS 258, 177
Fabian, A.C., Arnaud, K.A., Bautz, M.W., Tawara, Y., 1994, ApJ 436, L63
Fabian, A.C. 1994, ARS&A 32, 277
Fabian, A.C., Sandaers, J.S., Ettori, S., et al. 2000 submitted to MNRAS
Jones C., Forman W. 1984, ApJ, 276, 38
Fukazawa, Y. 1998, PhD thesis, University of Tokyo
Fukazawa, Y., Makishima, K., Tamura, T., et al. 2000, MNRAS, 313, 21
den Herder, J.W., et al. 2001, A&A, submitted. 1999, ApJ, 525, 58
Jansen, F., et al. 2001, A&A, submitted.
Johnstone, R.M., Fabian, A.C., Edge, A.C., Thomas, P.A., 1992, MNRAS 255, 431
Kaastra, J.S., Mewe, R., Nieuwenhuijzen, H., in UV and X-ray Spectroscopy of Astrophysical and Laboratory Plasmas, p. 411, eds. K. Yamashita and T. Watanabe, Tokyo, Univ. Ac. Press.
Kaastra, J.S., Ferrigno, C., Tamura, T., et al., 2001, A&A, submitted.
Matsumoto, H., Koyama, K., Awaki, H., et al., 1996, PASJ 48, 201
Mittaz, J.P.D., Kaastra, J.S., Tamura, T., et al. 2001, A&A, submitted.
Mewe, R., Kaastra, J.S., Liedahl, D.A., 1995, Legacy 6, 16
Peterson, J.R., Paerels, F.B.S., Kaastra, J.S., et al., 2001, A&A, submitted.
Phillips, K.J.H., Mewe, R., Harra-Murnion, L.K., et al., 1999, A&AS 138, 381
Turner, M., et al. 2001, A&A, submitted.
Xu, H., Makishima, K., Fukazawa, Y., 1998, ApJ 500, 738